



**HAL**  
open science

## Modelling flash flood propagation in urban areas using a two-dimensional numerical model

Kamal El Kadi Abderrezzak, André Paquier, Emmanuel Mignot

### ► To cite this version:

Kamal El Kadi Abderrezzak, André Paquier, Emmanuel Mignot. Modelling flash flood propagation in urban areas using a two-dimensional numerical model. *Natural Hazards*, 2009, 50, pp.433-460. 10.1007/s11069-008-9300-0 . hal-04651696

**HAL Id: hal-04651696**

**<https://hal.inrae.fr/hal-04651696v1>**

Submitted on 17 Jul 2024

**HAL** is a multi-disciplinary open access archive for the deposit and dissemination of scientific research documents, whether they are published or not. The documents may come from teaching and research institutions in France or abroad, or from public or private research centers.

L'archive ouverte pluridisciplinaire **HAL**, est destinée au dépôt et à la diffusion de documents scientifiques de niveau recherche, publiés ou non, émanant des établissements d'enseignement et de recherche français ou étrangers, des laboratoires publics ou privés.



Distributed under a Creative Commons Attribution - NonCommercial 4.0 International License

# Modelling flash flood propagation in urban areas using a two-dimensional numerical model

Kamal El Kadi Abderrezzak, André Paquier and Emmanuel Mignot

**Abstract** This paper reports on the numerical modelling of flash flood propagation in urban areas after an excessive rainfall event or dam/dyke break wave. A two-dimensional (2-D) depth-averaged shallow-water model is used, with a refined grid of quadrilaterals and triangles for representing the urban area topography. The 2-D shallow-water equations are solved using the explicit second-order scheme that is adapted from MUSCL approach. Four applications are described to demonstrate the potential benefits and limits of 2-D modelling: (i) laboratory experimental dam-break wave in the presence of an isolated building; (ii) flash flood over a physical model of the urbanized Toce river valley in Italy; (iii) flash flood in October 1988 at the city of Nîmes (France) and (iv) dam-break flood in October 1982 at the town of Sumacárcel (Spain). Computed flow depths and velocities compare well with recorded data, although for the experimental study on dam-break wave some discrepancies are observed around buildings, where the flow is strongly 3-D in character. The numerical simulations show that the flow depths and flood wave celerity are significantly affected by the presence of buildings in comparison with the original floodplain. Further, this study confirms the importance of topography and roughness coefficient for flood propagation simulation.

**Keywords** Urban flash flood · Shallow-water equations · 2-D depth-averaged model · Dam-break wave

K. El Kadi Abderrezzak (✉) · A. Paquier  
Cemagref, UR HHLY, 3bis quai Chauveau-CP220, F-69336 Lyon, France  
e-mail: kamal.elkadi@cemagref.fr; elkadi@lyon.cemagref.fr

A. Paquier  
e-mail: andre.paquier@cemagref.fr

E. Mignot  
LEGI, Laboratory of Geophysical and Industrial Fluid Flows,  
1025 rue de la Piscine BP 53, 38041 Grenoble Cedex 9, France  
e-mail: Emmanuel.Mignot@hmg.inpg.fr

## List of notations

$A$	Cell area
$C_r$	Courant number
$c$	Average wave celerity
$d_{i,j}$	Distance between the midpoint of the edge $(i, j)$ and one of the adjacent edges
$\mathbf{E}$	$x$ -Component of flux vector (Eq. 2)
$\bar{E}_{rr}$	Average relative error
$\mathbf{F}$	Flux vector = $[\mathbf{E}(\mathbf{U}), \mathbf{G}(\mathbf{U})]$
$g$	Gravitational acceleration
$\mathbf{G}$	$y$ -Component of flux vector (Eq. 2)
$H$	Flow depth
$I$	Cell index
$i, j$	Index for the edge between the cells $i$ and $j$
$K_s$	Strickler coefficient for flow resistance calculations (Eq. 3a, b)
$l$	Edge length
$n$	Time index
$N_i$	Set of neighbour cells of a cell
$\mathbf{n}$	Edge outside normal unit vector
$\mathbf{P}$	Transformation matrix (Eq. 7)
RMSE	Root mean square error
$\mathbf{S}$	Source term vector = $\mathbf{S}_0 + \mathbf{S}_f$
$\mathbf{S}_0$	Bottom slope vector
$\mathbf{S}_f$	Energy losses vector
$t$	Time
$u$	Flow velocity in the $x$ -direction
$\mathbf{U}$	Vector of conservative variables = $[h, hu, hv]^T$
$\mathbf{U}^L, \mathbf{U}^R$	Values of $\mathbf{U}$ at the left- and right-hand sides of an edge, respectively
$\mathbf{U}_x, \mathbf{U}_y$	Slopes of $\mathbf{U}$ over a cell in the $x$ - and $y$ -directions, respectively
$\alpha^{(x)}, \alpha^{(y)}$	$x$ - and $y$ -Components of the normal unit vector $\mathbf{n}$
$v$	Flow velocity in the $y$ -direction
$x, y$	Cartesian co-ordinates
$z_b$	Bed elevation
$z_w$	Water surface elevation
$z_w^*$	Average water surface elevation over a cell
$\Delta t$	Computational time step
$\eta, \xi$	Local coordinates
$\partial$	Partial derivative
$\nabla$	Divergence operator
	Posing that

## 1 Introduction and background

Flash floods can occur in urban areas after short-lasting severe rainfalls, causing substantial economic and social impacts (e.g. loss of human life, damage to property, disruption of services). Dam or dyke break, overloaded drainage systems, impervious ground surfaces and steep bottom gradients strongly contribute to urban flash floods. These latter are expected to increase due to persisting urbanization in flood-prone areas (Nirupama and

Simonovic 2007) and global climate change (IPCC 2001), which would increase the frequency and intensity of extreme rainfall events. In the past years, public awareness to extreme flood events increased, and water authorities would expect more information on flash-flood hazard conditions in urban areas. This problem may be dealt with through field observations, hydraulic modelling studies, or some combination of the two. In the absence of field observations, numerical modelling of flash-flood propagation may be used to explore extreme flood hazards (IMPACT 2004; Ikeda et al. 2008).

Many numerical models, mostly based on 1- or 2-D approaches, were developed to compute overland flows in urban areas. One-dimensional models are reasonably convenient to simulate flood propagation in straight streets, except near-street intersections where the flow is typically highly perturbed, and strongly 2-D or even 3-D (Neary et al. 1999). To compute the branching of the flow discharge at intersections, conceptual schemes and analytical relations were used (Nania et al. 2004). The main advantage of 1-D models is that they require less data, less computation time and computer memory than 2-D models. However, 1-D models ignore the details of hydraulic processes occurring at intersections and, more generally, in the extremely intricate network of streets and open spaces. Moreover, most 1-D models do not take into account flow paths around individual buildings, unless the layout and geometry of 1-D surface flow paths and ponds are generated automatically using advanced GIS tools (Djordjevic et al. 2007). Most published 1-D modelling studies concerned urban flooding caused by moderate rainfall and overflow of rivers or sewage system (Chowdhury 2000; Inoue et al. 2000; Mark et al. 2004; Djordjevic et al. 2005), but only few studies dealt with urban flash flooding attributed to high rainfall intensities and high flow velocities (Paquier et al. 2003; Lhomme et al. 2006).

To enhance the quality of urban flood hazard assessment, modellers generally support 2-D models (Ishigaki et al. 2004), as they are appropriate to simulate overland flow using a refined representation of topography and local hydraulic effects (e.g. complex flow patterns and abrupt hydraulic transitions). Two-dimensional models can provide data essential for risk assessment, such as flow depth and velocity vector at every grid point, which can be directly incorporated into mapping routines and/or GIS systems without interpolation. However, they require a lot of input data and a detailed bathymetry. Also, the use of complicated algorithms to treat source terms in the water governing equations often results in an excessively long computation time (Yoon and Kang 2004). Similar to 1-D models, most published 2-D numerical studies looked at scenarios of slowly rising flooding (e.g. Hsu et al. 2000; Aronica and Lanza 2005; Oberle and Merkel 2007). Only few 2-D numerical studies dealt with urban flash flooding (e.g. Paquier et al. 2003; Haider et al. 2003; Zenger and Wealands 2004; Mignot et al. 2006a, b).

Concerning urban modelling of flash floods, very few numerical models were successful in providing reliable results (Yu and Lane 2006), due to the absence of field measurements for model calibration and validation, the uncertainties associated with input data, and the extent of impervious surfaces as well as the complexity and variability of flow regimes. In this study, the extent to which a 2-D hydraulic model (Rubar20 code) can be applied to simulate flash flood propagation in urban areas is investigated. Laboratory tests were used for the assessment of model's accuracy, while two field cases were employed to investigate the effect of roughness and topography on flood propagation.

More in detail, a description of the 2-D numerical model Rubar20 is provided in Sect. 1. Section 2 is devoted to the validation of the model using various laboratory experimental cases, including a dam-break flow in the presence of an isolated building, and a flash flood event over the urbanized Toce river valley (Italy). In Sect. 3 the model is applied to simulate the catastrophic flood event that occurred in October 1988 at Nîmes (France), and

the flooding that occurred at Sumacárcel (Spain) in October 1982 after the failure of the Tous dam. Model predictions are compared to measurements in terms of flow depth and velocity. Finally, conclusions are drawn with the aim of providing some guidance to optimize 2-D flood modelling in urban areas.

## 2 Description of the modelling methodology using Rubar20 code

### 2.1 Governing equations

The 2-D model Rubar20 relies on the depth-averaged shallow-water equations. Disregarding the Coriolis, wind and viscous forces, these equations can be written in conservative and vector form as:

$$\frac{\partial \mathbf{U}}{\partial t} + \nabla \cdot \mathbf{F} = \mathbf{S} \quad (1)$$

where  $t$  = time,  $\mathbf{U}$  = vector of conservative variables,  $\mathbf{F} = \mathbf{F}(\mathbf{U}) = [\mathbf{E}(\mathbf{U}), \mathbf{G}(\mathbf{U})]$  = flux vector and  $\mathbf{S}$  = source terms vector.  $\mathbf{U}$ ,  $\mathbf{E}$ ,  $\mathbf{G}$  are defined as:

$$\mathbf{U} = [h, hu, hv]^T, \quad \mathbf{E} = \left[ hu, hu^2 + g \frac{h^2}{2}, huv \right]^T, \quad \mathbf{G} = \left[ hv, huv, hv^2 + g \frac{h^2}{2} \right]^T \quad (2)$$

and  $\mathbf{S} = \mathbf{S}_0 + \mathbf{S}_f$ , with  $\mathbf{S}_0$  as the bottom slope (Eq. 3a) and  $\mathbf{S}_f$  as the energy losses due to the bottom and wall shear stress.  $\mathbf{S}_f$  is computed using the Manning–Strickler law (Eq. 3b).

$$\mathbf{S}_0 = \left[ 0, -gh \frac{\partial z_b}{\partial x}, -gh \frac{\partial z_b}{\partial y} \right]^T \quad (3a)$$

$$\mathbf{S}_f = \left[ 0, g \frac{u \sqrt{u^2 + v^2}}{K_s^2 h^{1/3}}, g \frac{v \sqrt{u^2 + v^2}}{K_s^2 h^{1/3}} \right]^T \quad (3b)$$

where  $x$  and  $y$  = Cartesian co-ordinates,  $h$  = flow depth,  $u$  and  $v$  =  $x$ - and  $y$ -components of the velocity,  $g$  = gravitational acceleration,  $z_b$  = bed elevation and  $K_s$  = Strickler coefficient.

### 2.2 Grid mesh

A refined grid mesh with quadrilaterals and triangles was adopted to represent the urban area topography; the buildings were modelled as solid boundaries. The use of this grid provided various possibilities to adapt the model to particular details of urban topography, such as intersections and other structural features.

### 2.3 Numerical scheme algorithm

The non-linearity of the flux vector  $\mathbf{F}$  may lead to spontaneous hydraulic discontinuities having real physical meaning (e.g. hydraulic jumps, steep fronts, bores). Therefore, Eq. 1 was solved using an adaptation of the Monotonic Upstream Schemes for Conservation Laws (MUSCL) finite-volume method, which is a second-order accurate Godunov-type scheme (VanLeer 1979). This robust scheme is shock capturing, and describes the hydraulic discontinuities accurately (e.g. shock waves over initially dry bed, and transition

between subcritical and supercritical flows). Thus, it is particularly appropriate for simulating flood propagation in urban areas (Mingham and Causon 1998; Guinot and Soares-Frazão 2006).

In the model, the space is discretized into computational cells over which the average value of  $\mathbf{U}$  is computed at each time step (Fig. 1). The average value of  $\mathbf{U}$  over the cell  $i$  at the time level  $n$  is denoted by  $\mathbf{U}_i^n$ . The numerical scheme includes the following steps:

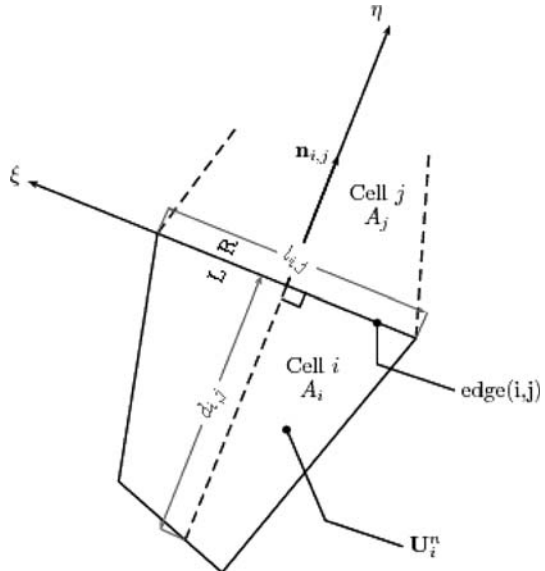
1. The slope of each component of  $\mathbf{U}$  (i.e.  $h$ ,  $hu$  and  $hv$ ) is computed at the time level  $n$ , at every grid cell  $i$ , in both  $x$ - and  $y$ -directions using the least squares method. Slopes are limited by a non-linear function called “minmod limiter” in order to avoid the generation of non-physical oscillations near discontinuities (Hirsch 1988). This function is defined using the total variation diminishing (TVD) property. The slopes of  $\mathbf{U}$  over the cell  $i$  at the time level  $n$  in  $x$ - and  $y$ -directions are denoted by  $\mathbf{U}_{x_i}^n$  and  $\mathbf{U}_{y_i}^n$ , respectively.
2. Values of  $\mathbf{U}_{i,j}^n$  at the middle of the edge  $(i, j)$  between cells  $i$  and  $j$  are computed at the time level  $n$  using the slopes obtained during the first step. Two values are obtained:  $\mathbf{U}_{i,j}^{nL}$  is calculated from the cell  $i$  and  $\mathbf{U}_{i,j}^{nR}$  is calculated from the cell  $j$ , with L and R as indexes referring to the left and right sides of the edge  $(i, j)$ , respectively.
3. On the basis of the slopes calculated in the first step and using an Euler time discretization  $\mathbf{U}_{i,j}^{n+1/2L}$  and  $\mathbf{U}_{i,j}^{n+1/2R}$  are computed as:

$$\mathbf{U}_{i,j}^{n+1/2L} = \mathbf{U}_{i,j}^{nL} - 0.5\Delta t \left( \frac{\partial \mathbf{E}}{\partial \mathbf{U}} \mathbf{U}_{x_i}^n + \frac{\partial \mathbf{G}}{\partial \mathbf{U}} \mathbf{U}_{y_i}^n \right) + 0.5\Delta t \mathbf{S}_i^n \quad (4)$$

$$\mathbf{U}_{i,j}^{n+1/2R} = \mathbf{U}_{i,j}^{nR} - 0.5\Delta t \left( \frac{\partial \mathbf{E}}{\partial \mathbf{U}} \mathbf{U}_{x_j}^n + \frac{\partial \mathbf{G}}{\partial \mathbf{U}} \mathbf{U}_{y_j}^n \right) + 0.5\Delta t \mathbf{S}_j^n \quad (5)$$

where  $\Delta t$  = time step, and  $\mathbf{S}_i^n$  = value of the source terms vector  $\mathbf{S}$  over the cell  $i$  at the time level  $n$ .

**Fig. 1** Sketch illustrating the finite volume discretization



4. Since values of  $\mathbf{U}_{i,j}^{n+1/2}$  at the middle of the edge  $(i, j)$  are generally different when computed from both left and right sides, a 1-D Riemann problem is considered at the time level  $n + 1/2$  in the direction normal to the edge  $(i, j)$ . The initial data at the time level  $n + 1/2$  is characterized by the two states  $\mathbf{U}_{i,j}^{n+1/2L}$  and  $\mathbf{U}_{i,j}^{n+1/2R}$ . The Riemann problem is solved in an approximate way using the well-known Roe-type linearization (Alcrudo and Garcia-Navarro 1993), thus obtaining one single value of  $\mathbf{U}_{i,j}^{n+1/2}$ .
5. The value of  $\mathbf{U}_i^{n+1}$  over the cell  $i$  at the time level  $n + 1$  reads:

$$\mathbf{U}_i^{n+1} = \mathbf{U}_i^n - \frac{\Delta t}{A_i} \sum_{j \in N_i} \mathbf{P}_{i,j} \mathbf{F}_{i,j}^{n+1/2} l_{i,j} + \Delta t \mathbf{S}_i^{n+1/2} \quad (6)$$

where  $A_i$  = area of the cell  $i$ ,  $l_{i,j}$  = length of the edge  $(i, j)$ ,  $\mathbf{F}_{i,j}^{n+1/2}$  = average value of  $\mathbf{F}$  in the direction normal to the interface  $(i, j)$  between the time levels  $n$  and  $n + 1$ ,  $N_i$  = set of the neighbouring cells of the cell  $i$ ,  $\mathbf{S}_i^{n+1/2}$  = average value of  $\mathbf{S}$  over the cell  $i$  between time levels  $n$  and  $n + 1$ , and  $\mathbf{P}_{i,j}$  = matrix that accounts for the coordinate change from the global coordinate system  $(x, y)$  to the local coordinate system  $(\eta, \zeta)$  attached to the edge  $(i, j)$ .  $\mathbf{P}_{i,j}$  is expressed as:

$$\mathbf{P}_{i,j} = \begin{bmatrix} 1 & 0 & 0 \\ 0 & \alpha_{i,j}^{(x)} & -\alpha_{i,j}^{(y)} \\ 0 & \alpha_{i,j}^{(y)} & \alpha_{i,j}^{(x)} \end{bmatrix} \quad (7)$$

where  $\alpha_{i,j}^{(x)}$  and  $\alpha_{i,j}^{(y)}$  =  $x$ - and  $y$ -components of the normal unit vector  $\mathbf{n}_{i,j}$  to the edge  $(i, j)$  (oriented positive from cell  $i$  towards cell  $j$ ).

## 2.4 Second member terms

The computation of the bottom slope source term  $\mathbf{S}_0$  (Eq. 3a) was not a trivial task, as the vertices of each cell do not usually lie on the same plane (Valiani et al. 2002). Various techniques were proposed in the literature to compute  $\mathbf{S}_0$  (Hubbard and Garcia-Navarro 2000). For example, Caleffi et al. (2003) split the cell in four sub-cells, and computed the bed slope over the cell as the weighted average of the slopes of the sub-cells. Bradford and Sanders (2002) assumed that bed slope varies bilinearly, and applied a  $2 \times 2$  Gauss quadrature to discretize  $\mathbf{S}_0$ . In Rubar20, a much more simple method was adopted. The term  $\mathbf{S}_0$  was treated as a flux so that a horizontal water surface remains horizontal. Noting with  $z_w$  the free-surface elevation, after some algebraic manipulation  $\mathbf{S}_0$  can be written as:

$$\mathbf{S}_0 = \begin{bmatrix} 0 \\ -gh \frac{\partial z_b}{\partial x} = \frac{\partial}{\partial x} \left( \frac{1}{2} gh^2 \right) \Big|_{z_w = \text{const} = z_w^*} \\ -gh \frac{\partial z_b}{\partial y} = \frac{\partial}{\partial y} \left( \frac{1}{2} gh^2 \right) \Big|_{z_w = \text{const} = z_w^*} \end{bmatrix} \quad (8)$$

in which  $z_w^*$  denotes the average water level in one cell, computed over the same interval as for the average flow depth  $h$ . Integrating over an arbitrary cell  $i$  of area  $A_i$ , and applying the Gauss theorem, Eq. 8 becomes:

$$\int_{A_i} \mathbf{S}_0 dA = \begin{bmatrix} 0 \\ -\sum_{j \in N_i} \frac{1}{2} g (z_{b,i,j} - z_{b,i}) (h_{i,j} + h_i) \alpha_{i,j}^{(x)} l_{i,j} \\ \sum_{j \in N_i} \frac{1}{2} g (z_{b,i,j} - z_{b,i}) (h_{i,j} + h_i) \alpha_{i,j}^{(y)} l_{i,j} \end{bmatrix}, \quad (9)$$

where  $z_{b,i}$  = average bed elevation over the cell  $i$ , computed at the gravity centre of the cell,  $z_{b,i,j}$  = bed elevation at the middle of edge  $(i, j)$ ,  $h_i$  = average flow depth over the cell  $i$  and  $h_{i,j}$  = flow depth in the middle of  $(i, j)$ .

The friction term  $\mathbf{S}_f$  (Eq. 3b) was assessed at the centre of the cell using a partially implicit scheme (Paquier 1995), in order to avoid numerical instabilities when rapid changes in flow depth or velocity occur.

## 2.5 Flooding/drying algorithm

During the computations, a cell was considered dry as long as the water volume in the cell induced a flow depth in the cell lower than a minimal value (0.001 mm in the present computations). In such case, the flow depth and velocity components in the cell were set to zero. Detailed numerical simulations showed that the mass conservation was satisfied within a cumulative error of the order of  $10^{-4}\%$  (Paquier 1998).

## 2.6 Stability of the numerical scheme

As the scheme is explicit, stability and convergence require that the time step is limited. The following Courant condition was used for each grid cell  $i$ :

$$\Delta t \leq C_r \min_{ij} \frac{d_{i,j}}{\sqrt{u_{i,j}^2 + v_{i,j}^2 + c_i}} \quad (10)$$

where  $C_r$  = Courant number ( $0 < C_r < 1$ ), set at 0.5 in the present computations,  $c_i = \sqrt{gh_i}$  = average wave celerity over the cell  $i$ , and  $d_{i,j}$  = distance between the mid-point of the edge  $(i, j)$  and one of the adjacent edges, calculated along the inward normal to the edge  $(i, j)$  (Fig. 1).

## 3 Model testing with laboratory data

As dynamic measurements during urban flash floods are rarely available, laboratory data were selected to validate the model. The data sets employed in this analysis derive from the broader study of urban flood propagation undertaken during the EU funded IMPACT project (IMPACT 2004).

### 3.1 Dam-break wave in presence of an isolated building

#### 3.1.1 Description of the experiment

The purpose of this laboratory experiment was to investigate the effects of a single building on dam-break wave propagation. The experiment was carried out in the laboratory of the



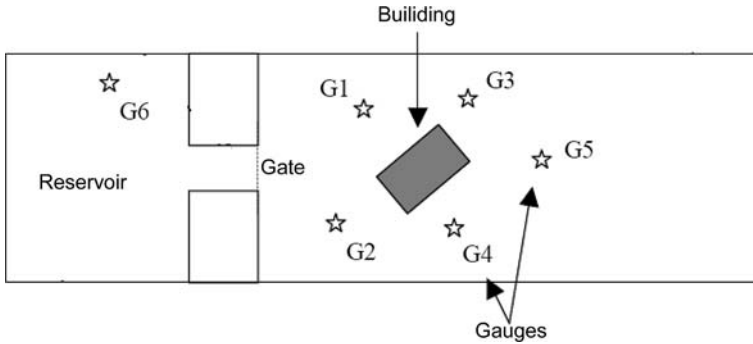


**Fig. 2** Dam-break wave in presence of an isolated building. Sketch illustrating the experimental set-up and position of the gauging points (G1–G6) where the flow depth was measured. Full description of the experiment is given in Soares-Frazão and Zech (2007)

Civil and Environmental Engineering Department at the Université Catholique de Louvain (UCL) in Belgium (Soares-Frazão and Zech 2007). The flume was horizontal, 35.80 m long and 3.6 m wide, with a partly trapezoidal cross-sectional shape near the bed (Fig. 2). A 1-m-wide rectangular gate was located between two fixed walls. A  $0.80 \times 0.40$  m rectangular building making an angle of  $64^\circ$  with the channel axis was fixed 3.40 m downstream from the gate. Initially, the water was set at rest in the 0.4-m-deep reservoir behind the gate, whilst a 0.01-m-thin water layer was set in the downstream reach. The flume had a smooth concrete bed, with a Strickler coefficient of approximately  $100 \text{ m}^{1/3} \text{ s}^{-1}$  (Soares-Frazão and Zech 2007). To simulate the dam-break wave, the gate was pulled up in approximately 0.25 s. The duration of the experiment was 30 s. Six gauges were used to measure the water level at different locations with a time step of 0.01 s (Fig. 2). The surface-velocity field was measured using a Voronoï imaging technique (Capart et al. 2002). A complete description of the laboratory experiment and available measurements can be found in Soares-Frazão and Zech (2007).

For the numerical simulations, the spatial domain was uniformly discretized using a space step of 0.05 m, resulting in 42,000 quadrilaterals and triangles. Two numerical simulations were performed: in the first simulation, the presence of the building was ignored; in the second simulation, the building was considered as an impervious area. The influence of the building on the dam-break wave propagation was therefore investigated. Simulations were carried out on a 3.2-GHz Intel EMT64 cluster station; the CPU time was about 3 h.

### 3.1.2 Global comparison

Figure 3 compares the measured and computed velocity fields at 1, 5 and 10 s after the dam break. At  $t = 1$  s, both computed (with and without building) and measured wavefronts form an elliptical shape downstream of the dam and reach the position  $x = 2.2$  m; this indicates that the calculated and measured flow waves move in the downstream direction approximately at the same celerity. At  $t = 5$  s, a noticeable impact of the building on the flood propagation can be appreciated (Fig. 3a, b), particularly in the vicinity of the obstacle. Indeed, velocities are reduced and more complex flow patterns can be observed: the hydraulic jumps, formed by the reflection of the wavefront against the building and the sidewalls of the channel, can be identified as the limits between high velocities upstream

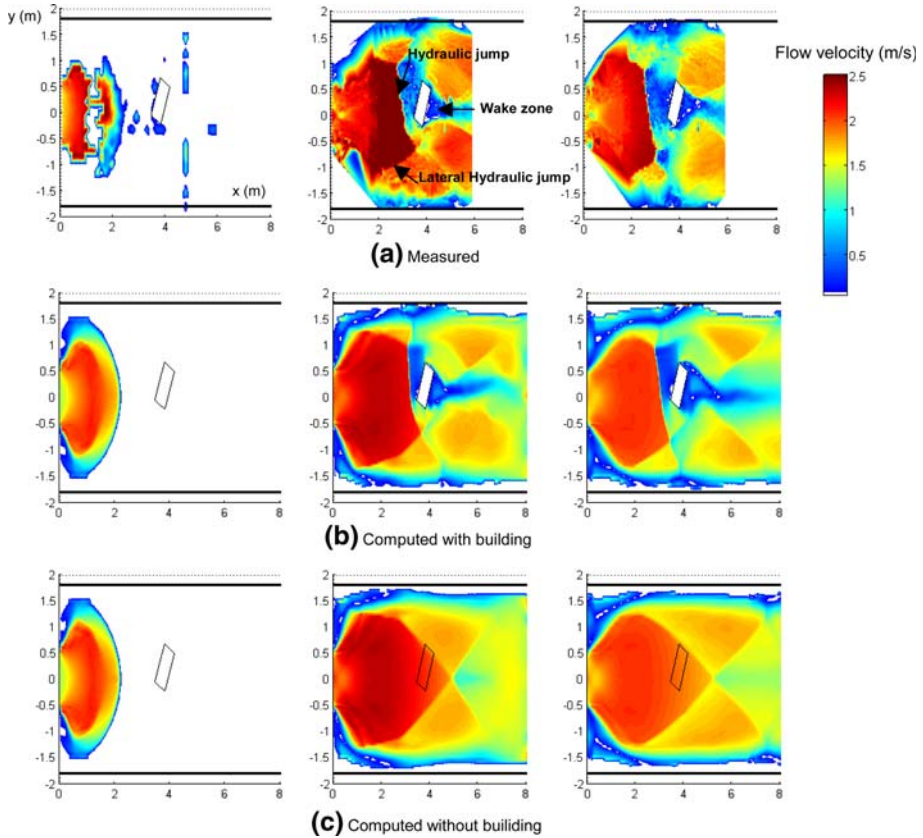


**Fig. 3** Dam-break wave in the presence of an isolated building. Computed and measured velocity fields immediately downstream of the gate at 1, 5 and 10 s after the dam break. **a** Measured. **b** Computed with building. **c** Computed without building. Note that measurements are not available for  $x > 6$  m. The origin of the axes is taken at the centre of the gate, with positive  $x$ -direction towards the downstream end of the channel

from the building and an area of water almost at rest. Also, a wake zone appears just behind the building. At  $t = 10$  s, velocities decrease; the lateral jump and wake zone remain but attenuate slightly, whilst the hydraulic jump formed by the reflection against the building propagates slowly in the upstream direction. The overall agreement between the model predictions and measurements is generally satisfactory when the building is taken into account: the flow structures appear both on the experimental data and the numerical predictions, at the same positions and with almost the same dimensions. However, some discrepancies in the velocity magnitude can be noted, particularly near the building and sidewalls, probably because of some additional local head losses caused by the reflection of the wave against the building and sidewalls, not accounted for in the numerical model.

### 3.1.3 Flow depth at selected gauges

Comparisons between the computed and measured flow depths at gauges G1, G4, G5 and G6 are presented in Fig. 4 (see Fig. 2 for gauge locations). The computed flow depths are

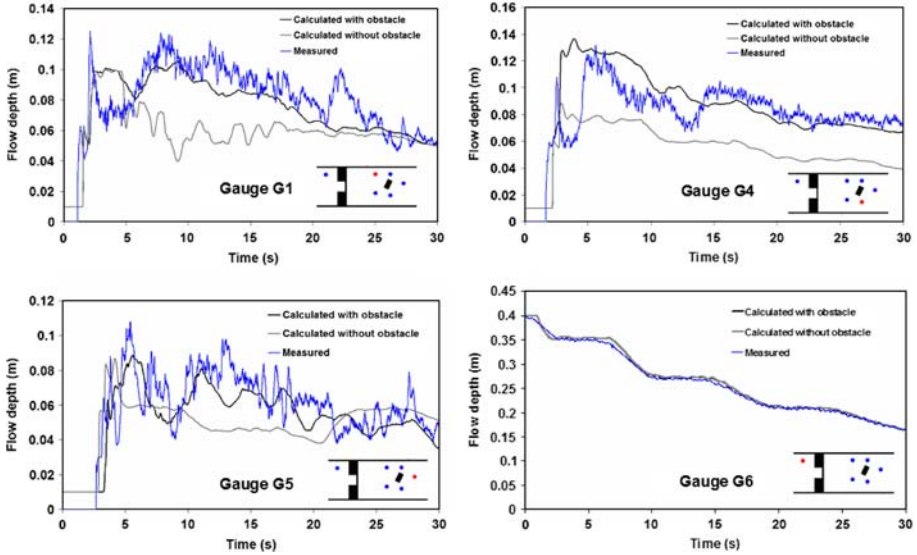


**Fig. 4** Dam-break wave in presence of an isolated building. Measured and computed flow depths at gauges G1, G4, G5 and G6. For gauge locations see Fig. 2

markedly increased at G1 and G4 when the building is taken into consideration, because of the backwater effects in front of the building and sidewalls. Similar increase can be observed at G5, except for the early times of the flooding ( $t < 5$  s) when the incoming water is partly blocked by the building. At times  $t > 20$  s, the influence of the building is limited in the downstream part of the channel (gauge G5), which suggests ignoring the building effects if only far field is of interest. The flow depth in the reservoir (gauge G6) is not influenced by the building, because the flow immediately downstream of the gate is supercritical.

Comparisons of the computed flow depths with the recorded data show that better agreement is obtained when the building is taken into account. At most of the gauge positions, acceptable estimates are obtained for the mean flow depth. The model reproduced the flow depth oscillations (G1, G4 and G5) reasonably well, although their amplitude and period were not accurately simulated. Finally, the flow depth in the reservoir (gauge G6) is reasonably well predicted. The root mean square error RMSE over the experiment duration (30 s), calculated as the 2nd moment of the difference between measured and computed flow depths at G1, G4, G5 and G6, is 0.011 m for the case with building, and 0.023 m for the case without building.

It is not surprising that some discrepancies between numerical predictions and experimental data were obtained. Indeed, the flow was highly 3-D near the building and the assumption of the hydrostatic pressure distribution in the governing equations was seriously compromised during the early times of the wavefront propagation and when water was strongly reflected against the building and the sidewalls. Also, the Manning–Strickler formula used to express the bottom friction may be inadequate for dam-break waves since it was originally derived for uniform-flow conditions (Soares-Frazão and Guinot 2007). All these aspects may explain the discrepancies between the computed and observed flow depths, particularly the amplitude and period of the flow depth oscillations recorded by the gauges, which were not accurately reproduced by the model.

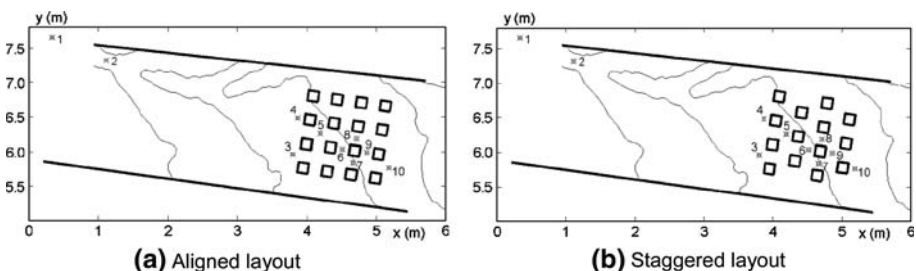
### 3.2 Physical model of the urbanized Toce river valley

A physical model of a city located within a narrow flood plain was built at ENEL (Milano, Italy) under the EU funded CADAM (1999) and IMPACT (2004) projects to study extreme flood events (Testa et al. 2007). A 5-km reach of the Toce river valley in Italy was scaled down 100 times to give the dimensions of  $50 \times 13$  m in the physical model. Cubic concrete blocks of 0.15 m length were implemented in the upstream reach of the scaled model, according to two distinct configurations: aligned or staggered (Fig. 5). In order to separate the effects of the valley topography from those caused solely by the urban district, two masonry walls were placed parallel to the model main axis, thus providing a channelling effect. The domain was initially dry and various inflow discharge hydrographs were tested. Water levels were measured with 0.2 s time step at 10 locations by means of gauges indicated by numbers 1,2,...,10 in Fig. 5.

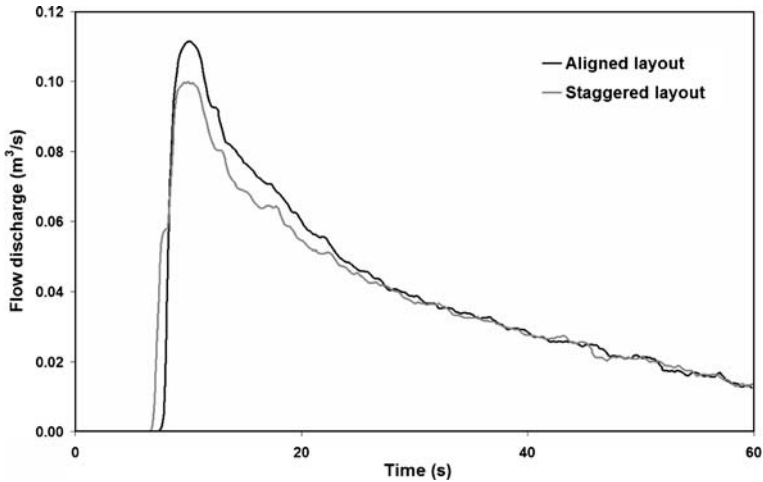
In the computations, only the 7-m-long region located at the upstream end of the physical model was simulated. The numerical grid was composed of 18,400 cells, with an average grid size of 0.03 m. The Strickler coefficient was set to  $62 \text{ m}^{1/3} \text{ s}^{-1}$ , as recommended by Testa et al. (2007). The measured inflow hydrographs for both configurations are shown in Fig. 6. These two flow discharge hydrographs are quite similar, although some differences can be observed for the flow peak. For both configurations, critical flow regime was assumed on the downstream boundary. Numerical runs lasted about 1.7 h on a 3.2 GHz Intel EMT64 cluster station.

Figure 7 shows snapshots of the simulated water surface elevation. Regardless of the city configuration, the urban district induced a reduction of the available flow section, which resulted in the formation of strong hydraulic jumps upstream of the buildings and in complex flow features (e.g. wake zones behind the buildings) inside the urban district (Fig. 7,  $t = 11.2$  and 12 s). As water progressed further downstream into the city, the flow became much more uniform, and the hydraulic jumps propagated in the upstream direction until their intensity decreased with time according to the inflow discharge (Fig. 7,  $t = 20$  s).

The computed stage-time hydrographs at gauges 4, 5, 6 and 10 are compared with measurements in Fig. 8. The overall trend of stage-time hydrographs was well reproduced although the model tended to overestimate the flow depth for the staggered layout case. The most significant differences were obtained at the gauges located close to the downstream end (e.g. gauge 10), where the boundary condition was difficult to determine. The flow was indeed so variable that the flow regime varied between subcritical and supercritical conditions along the downstream limit of the model, mainly because of the



**Fig. 5** Physical model of the urbanized Toce river valley. Topography of the valley and locations of the square blocks and gauging stations in the **a** aligned and **b** staggered configurations (from Testa et al. 2007). The contour line spacing is 0.005 m



**Fig. 6** Physical model of the urbanized Toce river valley. Measured experimental inflow hydrographs for aligned and staggered configurations, used as upstream boundary conditions in the numerical simulations

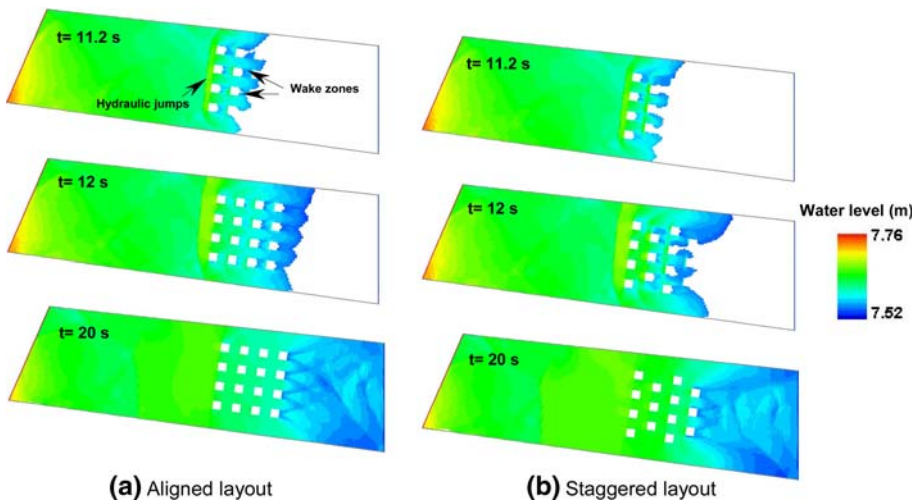


**Fig. 7** Physical model of the urbanized Toce river valley. Computed water elevation surface at different times. **a** Aligned layout. **b** Staggered layout

presence of wake zones behind the buildings. The root mean square error RMSE at stations 4, 5, 6 and 10 is 0.01 and 0.014 m for aligned and staggered configurations, respectively.

Assessing the influence of the arrangement of buildings on the flood propagation is an important subject for field studies. Then, an additional numerical simulation was performed for the staggered city layout using the inflow discharge hydrograph corresponding to the aligned layout case (Fig. 6). Generally, the aligned city layout exhibited less resistance to the flood propagation than the staggered one, thus inducing high flow velocity in the urban district. In terms of flow depth, the tendency was not the same because the second and fourth rows of buildings in the staggered city layout acted as important

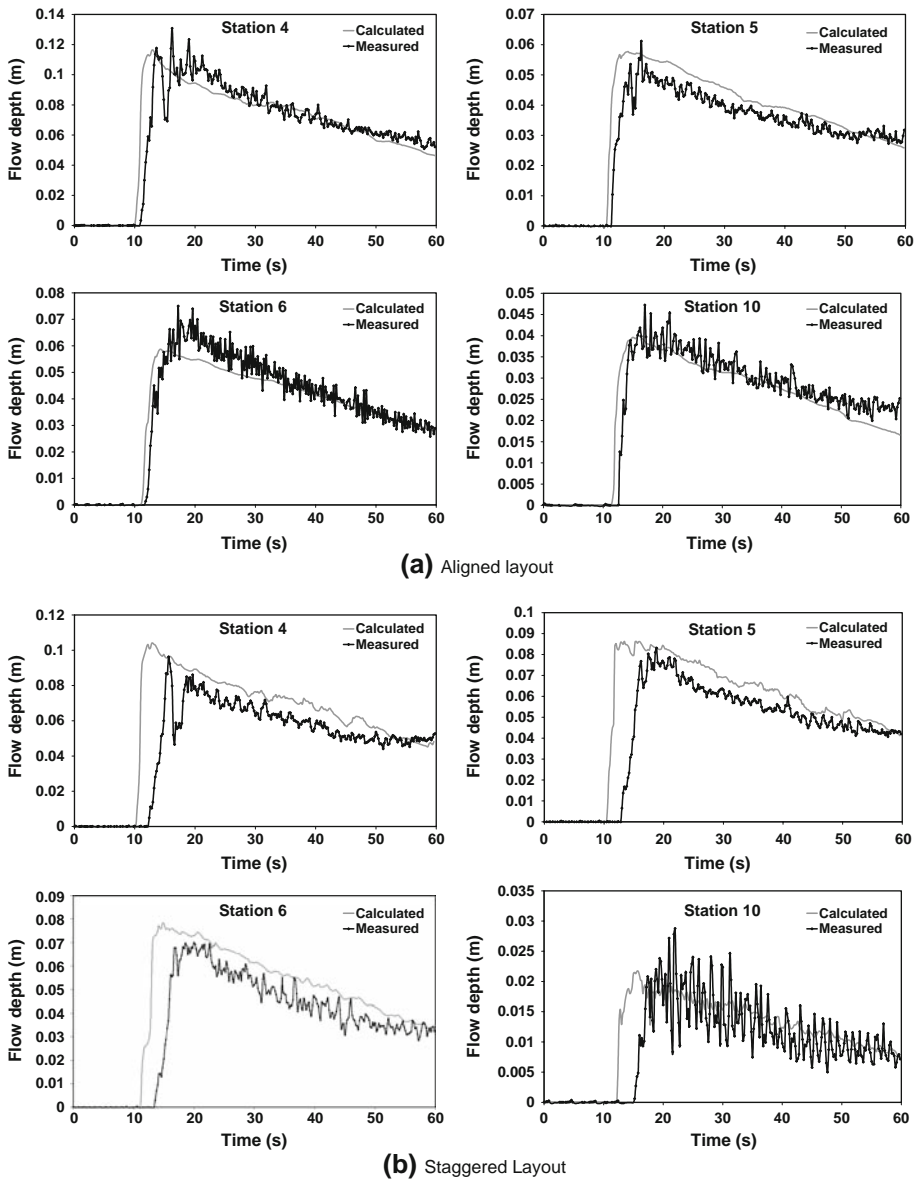


**Fig. 8** Physical model of the urbanized Toce river valley. Measured and computed flow depths at gauges 4, 5, 9 and 10. **a** Aligned layout. **b** Staggered layout. For gauge locations see Fig. 5

obstacles to the flow, thus increasing flow depth and decreasing velocities upstream of the buildings. A comparison was made in terms of flood intensity expressed by the product flow depth times velocity at  $t = 13.6$  s (this time corresponds to the peak values in the urban district). As shown in Fig. 9, results suggested that the staggered arrangement appears to induce a condition of higher severity, particularly inside the urban district.

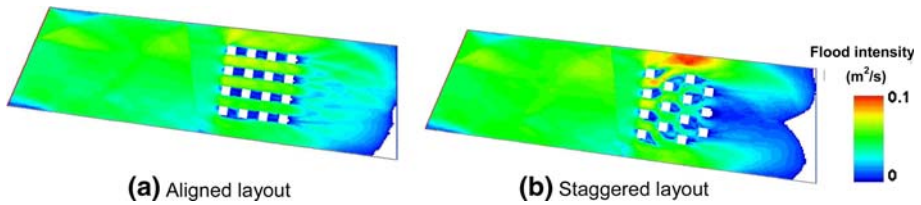


**Fig. 9** Physical model of the urbanized Toce river valley. Maps of flood intensity at  $t = 13.6$  s expressed by the product flow depth times velocity. **a** Aligned layout. **b** Staggered layout

## 4 Application to field cases

### 4.1 The October 1988 flood event in the city of Nîmes

Among the numerous floods that hit France during the last 20 years, the event that occurred on 3 October 1988 at the city of Nîmes was one of the most severe and dramatic (Fig. 10). The flood was caused by a heavy rainstorm that delivered 350 mm of precipitation in 3 h over the basin located immediately upstream of the city. The underground drainage system was rapidly saturated, and water flowed all over the streets, reaching in some locations a depth of 4 m, and causing ten casualties and damage of 50 million euros (Duclos et al. 1991). Desbordes et al. (1989) estimated the return period of this event to 150–250 years.



**Fig. 10** The Richelieu area of the city of Nîmes for which the 1988 flood event was simulated. S1–S11 denote the outlets of the domain

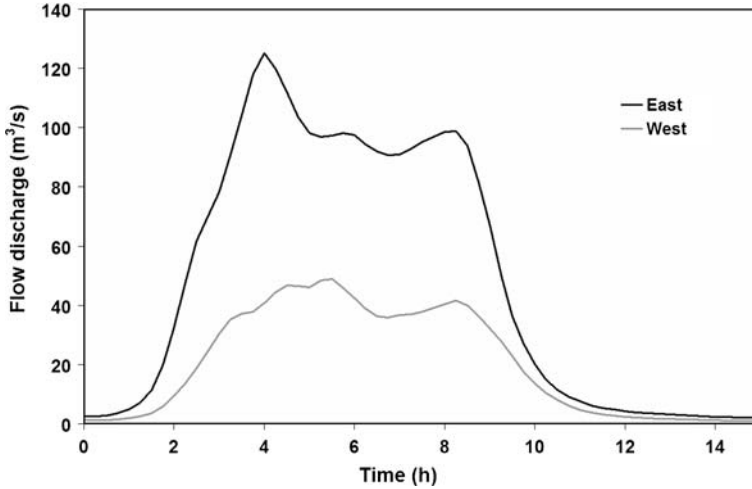


**Fig. 11** October 1988 flood event in the city of Nîmes. East and West inflow hydrographs of 100 years return period, used as upstream boundary conditions in the numerical simulations

The numerical model was applied to simulate this event in the Richelieu area, located in the north-eastern part of the city of Nîmes (Fig. 10), one of the most affected zones during the 1988 flood event. The upstream northern boundary conditions could be easily defined, as they are constituted by two structures crossing a railway embankment (Mignot et al. 2006b). Each of these two structures is fed by a small catchment for which the discharge hydrograph related to the 1988 flood was determined by BCEOM (2004) (Fig. 11). Both hydrographs were estimated using a hydrological model that relies on a conceptual linear tank approach similar to the GR4 model (Perrin et al. 2003), which considers separately the runoff from grasslands and urban zones. This model was calibrated considering the flow capacity of the structures crossing the railway embankment, and fitting the flood marks upstream from this railway embankment. The sewer network was taken into account by subtracting its discharge capacity from the calculated inflow hydrographs, but the sewer system capacities of less than  $4 \text{ m}^3 \text{ s}^{-1}$  were neglected.

The Richelieu area occupies  $1.2 \text{ km}^2$  of topographically rugged, steep slopes along the north-southern axis (higher than 1%). The northern part of the area includes large buildings (e.g. military barracks, hospital), wide streets and few crossroads. The central part includes residential zones, a regular narrow network (5–8 m wide) and street junctions with mainly  $90^\circ$  street angles. Street width in the southern part ranges between 10 and 20 m, with a steep slope in the north-southern direction.

#### 4.1.1 Data used for calculation

Two hundred cross sections were used to describe the 60 streets located in the Richelieu area. Cross-sectional profiles of the street junctions were obtained using a linear interpolation between the intersecting streets. A Digital Elevation Model (DEM) was processed using the set of cross sections and surface features (e.g. buildings, urban facilities). The computational mesh was generated from the DEM with an average space step of 25 m, which led the mesh generator to interpolate less than five additional cross sections along



each street. The grid mesh comprised about 42,000 cells, with 100 cells at each street intersection, and between 30 and 60 cells at each street.

The bottom friction is an effective quantity in flood modelling because it accounts for “sub-grid-scale” roughness of the terrain (Lane 2005). It may represent the lumped effects of several missing processes following calibration such as turbulence, dispersion of the horizontal velocities, presence of structural features as well as embankments and obstacles (Brown et al. 2005). In relation to urban floods, roughness parameterization becomes more complex because the required roughness values vary spatially as a function of local structural complexity. Various values of  $K_s$  were retained for 2-D flood modelling in urban areas: 13 (Calenda et al. 2003), 23 (Inoue et al. 2000), 40 (Gourbesville and Savioli 2002), 67 (Nania 1999) and  $100 \text{ m}^{1/3} \text{ s}^{-1}$  (Aronica and Lanza 2005). In this study, a Strickler coefficient of  $40 \text{ m}^{1/3} \text{ s}^{-1}$  was used; this value was considered representative of the predominantly smooth hard surfaces such as roads, paths and streets (Crowder et al. 2006). However, the central zone of the Richelieu includes narrow streets with many parked cars, which may generate a strong resistance to the flow. Thus, the Strickler coefficient in this zone (except the wide Faight and Semard streets) was reduced to  $20 \text{ m}^{1/3} \text{ s}^{-1}$ .

For the downstream boundary condition, the flow was assumed critical at the outlets S1 to S10, whilst a free outflow condition was imposed at the outlet S11 (Fig. 10). This condition was selected in order to take into account overflows to a railway line that is located 1 m downstream of the area boundary. The whole domain was assumed to be initially dry. Numerical runs lasted about 113.6 h on a 3.2-GHz Intel EMT64 cluster station.

#### *4.1.2 General results and comparison between numerical predictions and measurements*

The development of the predicted flow depths is shown in Fig. 12. Part of the eastern flow discharge turned towards the lower eastern part of the area, and left the domain through the exit S11 (Fig. 12,  $t = 0.20 \text{ h}$ ). However, a large part of both upstream floodwaters was rapidly moved to the Faight/Sully crossroad, travelling mainly along the narrow streets of the central zone before leaving the area at the southern limits. The domain was extensively flooded within 1 h (Fig. 12,  $t = 1 \text{ h}$ ). At the flood peak, high flow depths appeared at the eastern entry where the railway embankment blocked the water drainage area, and in the Faight street and Faight/Sully crossroad (Fig. 12,  $t = 4.1 \text{ h}$ ) where low velocities were calculated. High velocities ( $3\text{--}6.8 \text{ m s}^{-1}$ ) and supercritical regime flow (Fig. 13) was obtained along the main north-southern axis, whilst at street intersections the flow was generally complex, as both sub- and super-critical regimes developed. Finally, low velocities ( $0.5\text{--}0.7 \text{ m s}^{-1}$ ) with subcritical flow regime appeared in the streets oriented west-east.

Ninety-nine flood marks were recorded on the building walls, and were compared to the maximum flow depths calculated at the centres of the closest cells (Fig. 14). The average relative error  $\bar{E}_{\text{tr}}$  between the recorded and predicted peak flow depths was 42%, and the root mean square error RMSE over the entire domain was 0.46 m. Discrepancies were more pronounced at the eastern and western entries (“zones A and B”), in “zone C” due to a sudden narrowing of the Faight street width that may not be accurately represented in the interpolated mesh, and in “zone D” where the computed flow depths in the narrow streets were generally lower than the observed values by an average relative error of 28%, mainly due to the parked cars not explicitly represented in the model. In the southern area, the flow depth was slightly overestimated in a street located downstream of the Semard street (“zone E”).

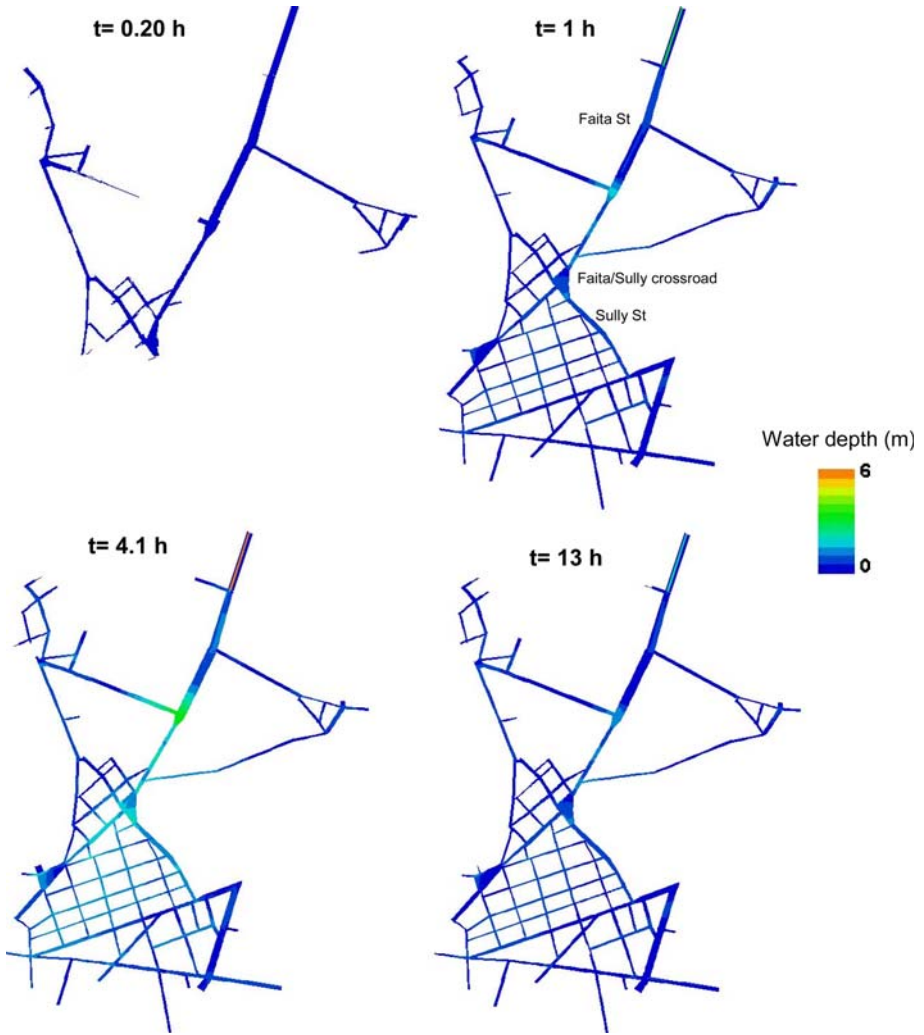


**Fig. 12** October 1988 flood event in the city of Nîmes. Computed flow depth field at different times

#### 4.1.3 Influence of the Strickler coefficient on the simulation results

To investigate quantitatively the influence of the Strickler coefficient on the numerical predictions, three additional simulations were carried out using different values of  $K_s$ . Table 1 summarizes the comparison between the predicted flood depths and flood marks in terms of  $\bar{E}_r$  and RMSE. For brevity, only results obtained with two simulations are presented here: (i) “Nîmes-1” simulation, for which the Strickler coefficient was set to  $10 \text{ m}^{1/3} \text{ s}^{-1}$  in the central zone (except the wide streets of Faighta and Semard) instead of  $20 \text{ m}^{1/3} \text{ s}^{-1}$  as used in the previous simulation (referred to as “Ref”); (ii) “Nîmes-2” simulation, for which the Strickler coefficient was increased to  $40 \text{ m}^{1/3} \text{ s}^{-1}$  in the central zone (except the wide streets of Faighta and Semard).

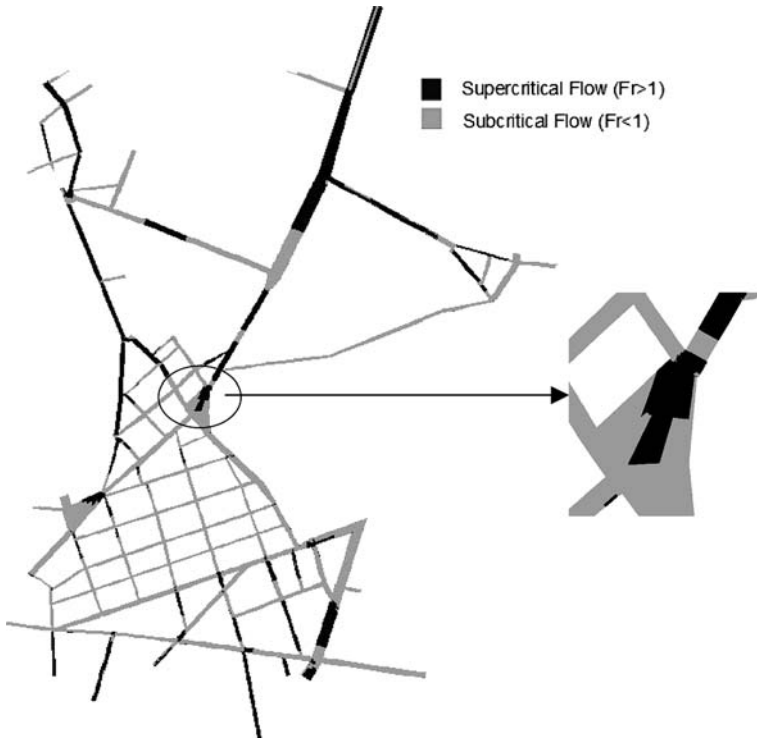


**Fig. 13** October 1988 flood event in the city of Nîmes. Computed flow regime field at the flood peak ( $t = 4.1$  h)

Compared to the “Ref” simulation, decreasing (“Nîmes-1” simulation) or increasing (“Nîmes-2” simulation) the Strickler coefficient of the central zone did not affect the flow depth field in the northern zone significantly. A more pronounced effect was obtained in the central zone and its neighbouring streets, as shown in Fig. 15. In the simulation “Nîmes-1,” the flow depth was significantly increased in some streets of the central zone ( $\Delta h < 0$  in Fig. 15a), while the flow depth decreased in the south-eastern area, between Semard and Beaucaire streets ( $\Delta h > 0$  in Fig. 15a) and, to a lesser extent, upstream of the central zone. An opposite trend was obtained with the simulation “Nîmes-2” (Fig. 15b). On the other hand, changing the Strickler coefficient modified the flow structures in most streets of the central zone. Moreover, in some streets and intersections, the flow regime changed from supercritical to subcritical conditions or vice versa (Fig. 16). This may explain the strong modification of the local flow depths shown in Fig. 15. However, the distribution of the flow discharge through the downstream boundary streets is hardly changed.

On the basis of  $\bar{E}_{rr}$  and RMSE, better results were obtained with the “Ref” simulation (Table 1). Using a uniformly distributed Strickler increased the average relative error and the root mean square error (e.g.  $\bar{E}_{rr} = 48\%$ , RMSE = 0.56 m “Nîmes-2” instead of  $\bar{E}_{rr} = 42\%$  and RMSE = 0.46 m “Ref”).

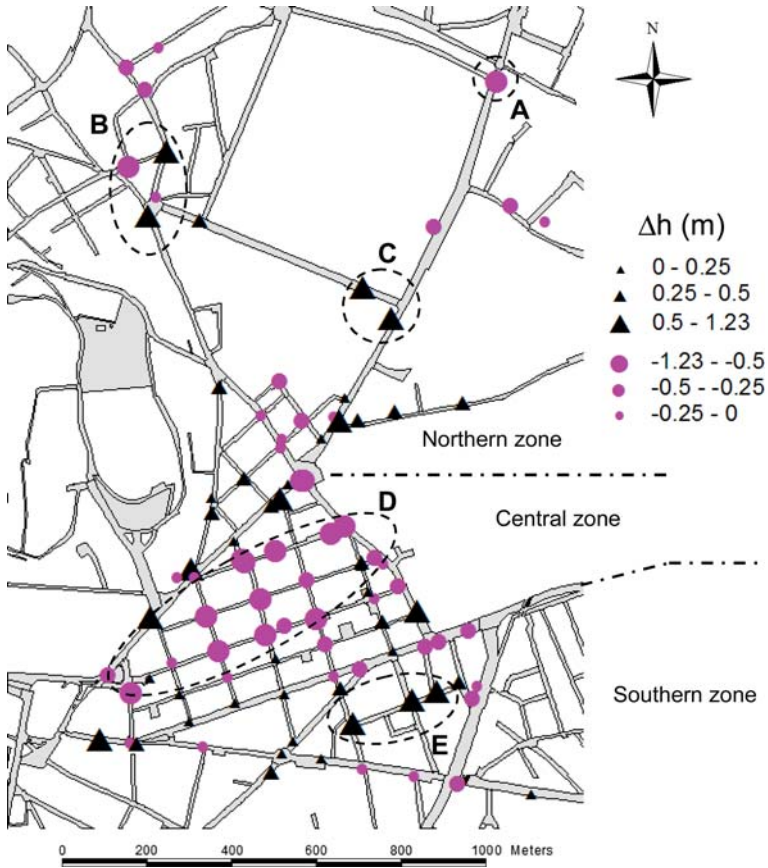


**Fig. 14** October 1988 flood event in the city of Nîmes. Comparison between maximum computed peak flow depths and measured flood marks ( $\Delta h = h_{\text{computed}} - h_{\text{measured}}$ )

**Table 1** October 1988 flood event in the city of Nîmes

Simulations	Ref	Nîmes-1	Nîmes-2	Nîmes-3
$K_s$ (central zone <sup>a</sup> )/ $K_s$ (rest of the domain)	20/40	10/40	40/40	30/30
$\bar{E}_{rr}$ (%)	42	47	48	46
RMSE (m)	0.46	0.53	0.56	0.53

Sensitivity analysis to the Strickler coefficient. Comparison between the simulated flood depths and flood marks

<sup>a</sup> Except the wide Faight and Semard streets

#### 4.2 Tous dam-break event

Tous dam is the most downstream flood control structure of the Júcar river basin in the central part of the Mediterranean coast of Spain (Fig. 17). On 20 and 21 October 1982 extremely heavy rainfalls fell over the Tous dam catchment (area of 17,820 km<sup>2</sup>), with an average depth of 500 mm. The total rainfall volume over the basin reached

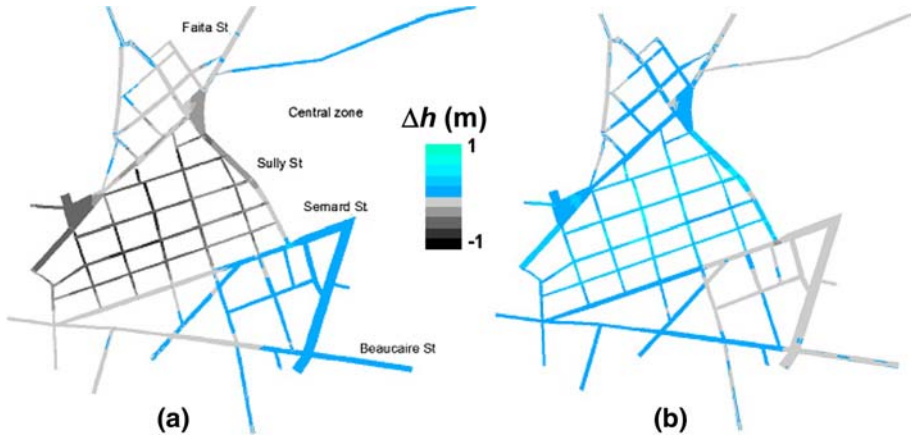


**Fig. 15** October 1988 flood event in the city of Nîmes. Changes in flow depth in the central zone at peak flow obtained with **a** Nîmes-1 and **b** Nîmes-2 simulations.  $\Delta h$  is calculated between the Ref and Nîmes-1 or Nîmes-2 simulation predictions (i.e.  $\Delta h = h_{\text{Ref}} - h_{\text{Nîmes-1,-2}}$ )

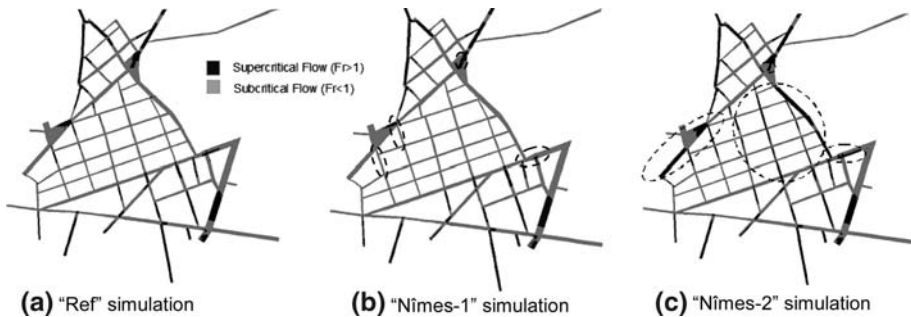


**Fig. 16** October 1988 flood event in the city of Nîmes. Computed flow regime fields at the flood peak ( $t = 4.1$  h) for, **a** Ref, **b** Nîmes-1 and **c** Nîmes-2 simulations. Dashed contours show the area where the flow regime is locally changed, thus affecting the local flow depth significantly

almost 600 million  $\text{m}^3$ , largely exceeding the storage capacity of the Tous reservoir (120 million  $\text{m}^3$ ). At 19:00 on October 20, the Tous dam failed, giving rise to a flooding wave that reached the cities located downstream of the dam, and drastically changing the Júcar valley morphology. The consequences of this event were catastrophic: 300  $\text{km}^2$  of inhabited land were flooded severely; some 200,000 people were affected and eight casualties were recorded. One of the most affected cities was the small town of Sumacárcel, located about 5 km downstream of the dam. The topography of the town is mountainous and most of the buildings lie on a steep slope terrain, which protected them from the river flow overtopping. However, the older part of the town is located closer to the right bank of a meander of the Júcar river. Thus, it was completely flooded on 20 October 1982, with flow depth reaching 6–7 m at some locations.

The numerical model was applied to simulate the October 1982 dam-break wave along the Júcar river valley, from upstream of the Tous dam to downstream of the Sumacárcel town (i.e. 8 km of the valley were modelled). The flooding of this town is a typical example of an extreme inundation that encompasses both flood propagation along natural



**Fig. 17** Location of the Júcar river valley with aerial view from the Tous dam to Sumacárcel city about one week after the dam break (after Alcrudo and Mulet 2007)

topography (i.e. the Júcar river valley) and subsequent inundation of an urban area (i.e. Sumacárcel town). This case was selected as a benchmark study for the flood propagation workpackage under the EU funded IMPACT project (IMPACT 2004). A complete description of the case study and of the data can be found in Alcrudo and Mulet (2007).

#### 4.2.1 Data used for calculation

Accurate topographic data prior to the Tous dam-break wave are not available for the Júcar river valley. Two Digital Terrain Models (DTM) with 5 m spatial resolution were realized after this event: the first one (referred to hereafter as 1982 DTM) dates few weeks after the dam break, while the second one (referred to hereafter as 1998 DTM) dates back to 1998, i.e. after the construction of the new Tous dam in 1995. Comparison of the 1982 and 1998 DTMs evidenced notable changes in the valley topography, with sediment deposition in the river bed, and erosion of river banks. These changes may be mainly attributed to the dredging work that was undertaken during the construction of the new Tous dam, and to the sediment transport that took place after the 1982 flood event (Alcrudo and Mulet 2007).

In this study, both 1982 and 1998 DTMs were used, thus allowing the investigation of the influence of the Júcar river valley topography on the extent of inundation zone and water levels in the Sumacárcel town after the Tous dam-break. The flow discharge hydrograph at the Tous dam was estimated by CEDEX (1989) using field observations, measurements in a 1:50 scale physical model of the Tous dam and its downstream reach, as well as hydrologic and hydraulic calculations. The flow discharge hydrograph spanned a period of about 2 days with a peak discharge of  $15000 \text{ m}^3 \text{ s}^{-1}$  (Fig. 18). However, it should be noted that the peak discharge occurred at 20:00 on October 20, with an abrupt increase between 19:00 and 20:00, which is in contradiction with field observations

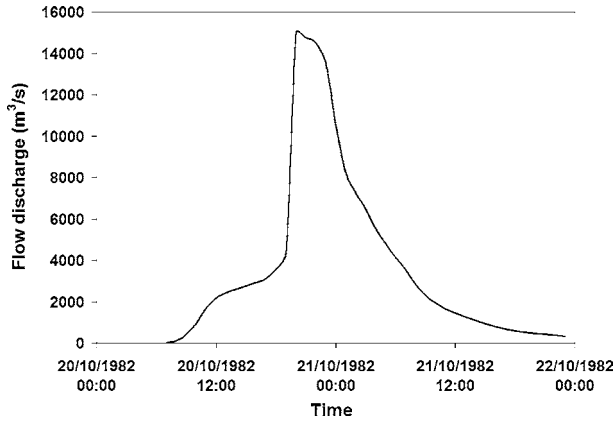


**Fig. 18** October 1982 Tous dam-break event. Inflow hydrographs injected at the upstream boundary of Júcar river valley

revealing that maximum water levels in the Sumacárcel town were attained at 19:40. Since peak-flooding levels should occur after the peak flow discharge and not the opposite, it is evident that the timing of the peak discharge as estimated by CEDEX (1989) could be erroneous.

Given the diversity of soils, vegetation coverage and crop fields present in the area under consideration, it is clear that the roughness varies substantially all over the domain. Of particular interest, the areas covered with orange trees appear to have a large influence on the flood propagation, by slowing down significantly the flow velocity. These areas located near the town were represented in the numerical computations as areas with a higher friction coefficient, corresponding to a Strickler coefficient of  $10 \text{ m}^{1/3} \text{ s}^{-1}$ . For the rest of the domain, a Strickler coefficient of  $33 \text{ m}^{1/3} \text{ s}^{-1}$  was retained, as recommended by Alcrudo and Mulet (2007). In the computations, a dry bed condition was initially imposed; therefore, the flow discharge in the Júcar river immediately before the failure of the dam was neglected. For the downstream boundary condition, the flow was assumed critical.

Due to the size of the valley (about 8 km long, and 1 km wide) and duration of the October 1982 flood event (about 2 days), a single calculation involving the whole valley and town would need a long computation time to be performed. Thus, it was decided to split the simulation of the Tous dam-break event into two sets of calculations: on each bathymetry, a preliminary simulation of the flood event over the whole valley (river and the old part of the town) was carried out using a coarse grid mesh and, as upstream boundary condition, the flow discharge hydrograph shown in Fig. 18. In order to obtain more detailed results for the flow propagation in the urban area, a second simulation was performed in a shorter reach of the valley including the older part of the Sumacárcel town: a refined mesh was used to describe the urban area topography, and the upstream boundary of the domain was obtained from the preliminary simulation.

In the preliminary simulations, the urban area was simplified by taking into account only the main streets of the town and by merging some buildings. The density of the mesh in the urban area was as coarse as possible, i.e. only one cell was used in each street and each intersection. The grid mesh over the whole valley comprised about 2600 cells for both 1982 and 1998 bathymetries. In the simulations performed with the refined mesh, the upstream limit of the domain was located at a section just upstream from the town, and the

downstream limit of the domain was located 400 metres downstream from the urban area. In terms of mesh density within the urban area, 9–16 cells were used in each street, whilst the number of cells at some intersections could be as high as 20 cells. In total, a grid mesh of 11,000 cells was used to represent the restricted reach of the valley with both 1982 and 1998 bathymetries. Simulations were carried out on a 3.2 GHz Intel EMT64 cluster station, and the CPU time for runs with the 1982 and 1998 bathymetries was 115.6 and 59.8 h, respectively.

#### 4.2.2 General results and comparison of numerical predictions with observations

For both bathymetries, the preliminary simulations showed that differences between the hydrograph at dam site and the one recorded just upstream from the urban area are not significant. Indeed, both flow discharge hydrographs have almost the same shape, and the peak discharge estimated at the dam-break location ( $15,000 \text{ m}^3 \text{ s}^{-1}$ ) is reduced by 2.5% only upstream of the Sumacárcel town.

The predicted maximum flood extents obtained using the refined mesh are shown in Fig. 19. Water overflowed the Júcar river banks extensively, flooding the town and reaching depths of up to 8 m at some locations. The extent maps are similar, even though the computed flow depths in the urban area with the 1982 bathymetry are higher. Finally, the differences in water elevations between the upper and lower part of the urban area are less than 0.12 cm in both runs, indicating that the town of Sumacárcel was not subject to the impact of an inertial flood although the dam break was an extreme flood event. This conclusion is supported by the findings of the IMPACT project (Alcrudo and Mulet 2004).

Maximum water elevation marks were recorded at 21 locations within or close to the Sumacárcel town (Fig. 20). Figure 21 compares the predicted water elevations and measurements. Quite large differences can be observed at most gauging points, depending on the bathymetry data set used in the numerical simulation. Observed differences of about 0.9–1.4 m can mainly be attributed to the differences between the 1982 and 1998 DTMs. The computed water elevations obtained with the 1982 bathymetry are generally higher than the field flood marks with an average value of 1.4 m, probably because of the

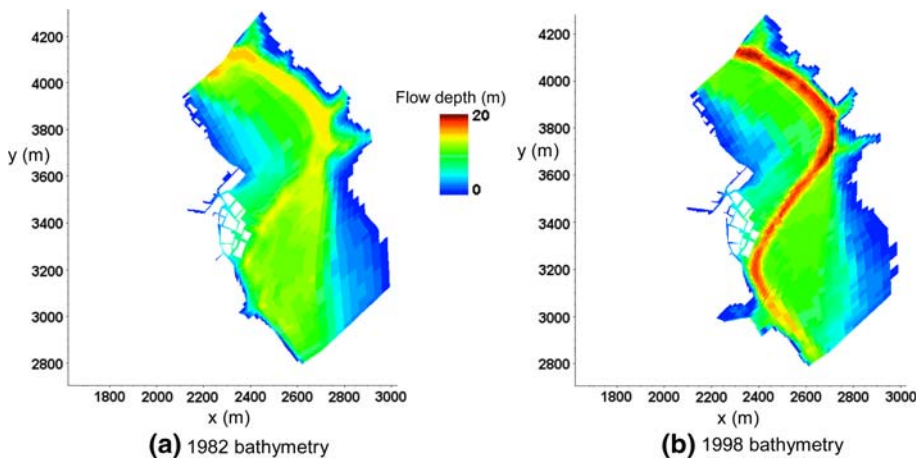


**Fig. 19** October 1982 Tous dam-break event. Computed maximum flood extents obtained using the refined mesh, with **a** 1982 bathymetry and **b** 1998 bathymetry



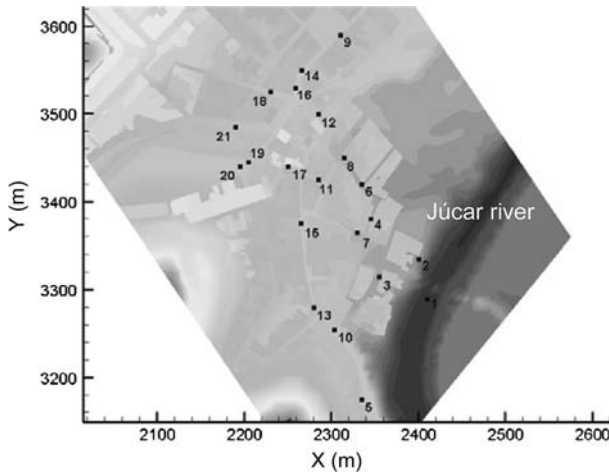


**Fig. 20** October 1982 Tous dam-break event. Locations of the gauges in the streets of Sumacárcel twon (after Alcrudo and Mulet 2007)

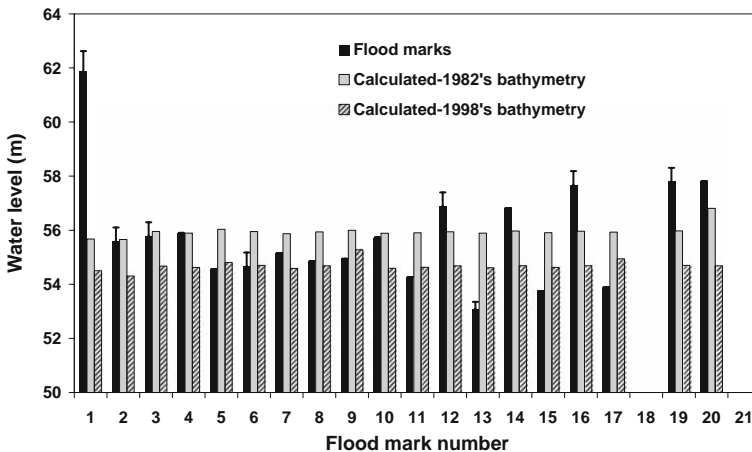


**Fig. 21** October 1982 Tous dam-break event. Comparison between maximum computed peak water levels and measured water elevation marks. The error bars represent the uncertainty in the field data, as estimated by Alcrudo and Mulet (2007)

sediment deposition that took place in the river bed just after the dam-break wave. The simulated water levels with the 1998 bathymetry are generally lower than the measured values, with an average value of 1.7 m, probably due to the deepening of the river bed after the dredging works carried out between 1982 and 1995. The maximum difference between the predictions and measurements can be observed at gauge 1, probably because of its closeness to the upstream boundary of the model, where the inflow condition might include non-negligible uncertainties (Mulet and Alcrudo 2003). Note that gauges 18 and 21 showed no flooding (zero or nearly zero flow depth).

## 5 Conclusions and recommendations

A 2-D model for studying flash flood propagation in urban areas was presented and tested. The 2-D shallow-water equations were solved using an explicit second-order numerical scheme that is adapted from MUSCL approach. A refined computational mesh, composed of quadrilaterals and triangles, was employed to represent the urban area topography, whilst building edges were modelled as solid boundaries. First, a set of laboratory cases representative of severe urban flood events was used to quantify the relevancy of the 2-D model. On the experimental study on dam-break wave in the presence of an isolated building, the numerical model predicted the general flow dynamics (i.e. flow depth changes and velocity field) following the dam-break wave with fair accuracy. Some discrepancies were observed between the numerical results and measurements near the building: in such location the flow was highly 3-D and the assumption of the hydrostatic pressure distribution in the 2-D shallow-water equations was not valid because of water reflection against the obstacle. An additional source of these discrepancies could be found in the Manning-Strickler formula used to compute the bottom friction; this formula may not be appropriate for dam-break waves since it was originally established for uniform-flow conditions. The influence of a single building on the wavefront propagation was also investigated. The flow pattern was deeply modified in the near-zone of the building, whilst the far field was less influenced by the presence of the obstacle, suggesting that this effect can be ignored if only the far field is under consideration.

In a second step, the capacity of the model to simulate urban flash flooding was verified using the physical model of the urbanized Toce river valley. The satisfactory agreement between the predicted and measured flow depths at selected gauge stations for both aligned and staggered city layouts confirmed the reliability of the model. The influence of the arrangement of buildings on the flood propagation was assessed, and it was found that the staggered configuration induced a higher intensity than the aligned configuration, particularly inside the urban district. This finding is compatible with the “flood-planned city concept” (Marco and Cayuela 1994).

Finally, the model was tested on the October 1988 flood event in the dense city of Nîmes and the October 1982 dam-break flood in the town of Sumacárcel. For the case of Nîmes city, the numerical simulations showed that more accurate predictions of flow depth can be obtained when a non-uniformly distributed Strickler coefficient is used. This finding confirmed that the selection of an appropriate Strickler coefficient for simulating flood propagation in urban areas is a relevant issue. The average relative error between the flood marks and predicted flow depths, and the root mean square error (42% and 0.46 m, respectively) were rather high, but flood marks may not reflect what actually occurred. Photos taken during the flood event showed in fact that the water surface rose along a few buildings irregularly due to the presence of waves. This induced serious uncertainties in the measurements, confirmed by comparing couples of close flood marks (Mignot 2005). In addition, topographical data may include non-negligible uncertainties. Flow depth deviations larger than 0.50 m constitute 28% of the flood marks. If these deviations were excluded, for the remaining flood marks (72%) the root mean square error decreased to 0.18 m, which is less than the expected error of 0.25 m from terrain elevations generated from the DTM. The results for the Tous dam-break case showed that, although the dam break was an extreme flood event, the town of Sumacárcel itself was not subject to the impact of an inertial flood. The computed water elevations obtained with the 1982 DTM (recorded a few weeks after the flood) were generally higher than the field flood marks, because the ground level was higher than the original one (prior to the dam break); on the

other hand the numerical results for the 1998 bathymetry were generally lower than the measurements, due to the deepening of the river bed during the dredging works between 1982 and 1995.

The results presented in this paper appear to be sufficiently encouraging to warrant further development of 2-D flow modelling as a worthwhile approach for simulating flash flood propagation in urban areas. Nevertheless, they also draw attention to required improvements in model parameter estimation (e.g. Strickler coefficient) and terrain data. Particularly, the effect of sediment transport on river bed changes has to be considered when urban flooding is attributed to some extreme natural events such as dam-break wave.

**Acknowledgements** The authors wish to acknowledge the financial support offered by the French National Research Agency (ANR) for Research Contract ANR-05-PGCU-004, "RIVES." Dr. Sandra Soares-Frazaõ and Professor Yves Zech (Université Catholique de Louvain), Guido Testa and David Zuccalà (CESI, Milan), Professor Francisco Alcrudo and Jonatan Mulet (Universidad de Zaragoza) are gratefully acknowledged for the work concerning the availability of experimental and field data. Finally, the authors would like to thank the guest editor (G. Iovine) and three anonymous reviewers for their detailed review and improvement of the English language of the original manuscript.

## References

- Alcrudo F, Garcia-Navarro P (1993) A high resolution Godunov-type scheme in finite volumes for the 2D shallow-water equations. *Int J Numer Methods Fluids* 16(6):489–505. doi:10.1002/flid.1650160604
- Alcrudo F, Mulet J (2004) Conclusions and recommendations from the IMPACT Project WP3: flood propagation. Available via [http://www.samui.co.uk/impact-project/AnnexII\\_DetailedTechnicalReports/AnnexII\\_PartB\\_WP3/WP3\\_10Summary\\_v1\\_0.pdf](http://www.samui.co.uk/impact-project/AnnexII_DetailedTechnicalReports/AnnexII_PartB_WP3/WP3_10Summary_v1_0.pdf)
- Alcrudo F, Mulet J (2007) Description of the Tous dam-break case study (Spain). *J Hydraul Res* 45(extra issue):45–57
- Aronica GT, Lanza LG (2005) Drainage efficiency in urban areas: a case study. *Hydrol Process* 19(5): 1105–1119. doi:10.1002/hyp.5648
- BCEOM CS, Metéo France (2004) Outil de prévision hydrométéorologique-Projet Espada-Ville de Nîmes. Bureau Central d'Etudes pour les Equipements d'Outre-Mer (BCEOM) Technical Report, France
- Bradford SF, Sanders BF (2002) Finite-volume model for shallow-water flooding of arbitrary topography. *J Hydraul Eng* 128(3):289–298. doi:10.1061/(ASCE)0733-9429(2002)128:3(289)
- Brown JD, Spencer T, Moeller I (2005) Modeling storm surge flooding of an urban area with particular reference to modeling uncertainties: a case study of Canvey Island, United Kingdom. *Water Resour Res* 43:W06402. doi:10.1029/2005WR004597
- CADAM (Concerted Action on Dam-break Modeling) (1999) Proceedings of the 3rd CADAM Meeting. Available via <http://www.hrwallingford.co.uk/projects/CADAM/CADAM/index.html>
- Caleffi V, Valiani A, Zanni A (2003) Finite volume method for simulating extreme flood events in natural channels. *J Hydraul Res* 41(2):167–177
- Calenda G, Calvani L, Mancini CP (2003) Simulation of the great flood of December 1870 in Rome. *Water Marit Eng* 156(4):305–312. doi:10.1680/maen.156.4.305.37926
- Capart H, Young DL, Zech Y (2002) Voronoï imaging methods for the measurements of granular flows. *Exp Fluids* 32(21):121–135. doi:10.1007/s003480200013
- CEDEX (1989) Revisión del estudio hidrológico de la crecida ocurrida en los días 20 y 21 de Octubre de 1982 en la Cuenca del Júcar. Centro de Estudios y Experimentación de Obras Públicas (CEDEX) Technical report, Spain
- Chowdhury MD (2000) An assessment of flood forecasting in Bangladesh: the experience of the 1998 flood. *Nat Hazards* 22(2):139–163. doi:10.1023/A:1008151023157
- Crowder R, van der Leer D, Burbidge J (2006) Integrated catchment & urban modelling for flood management. Available via <http://www.halcrow.com/software/>
- Desbordes M, Durepaire P, Gilly JC, Masson JM, Maurin Y (1989) 3 Octobre 1988-Inondations sur Nîmes et sa Région-Manifestations, Causes et Conséquences. Lacour, Nîmes
- Djordjevic S, Prodanovic D, Maksimovic C, Ivetic M, Savic D (2005) SIPSON-simulation of interaction between pipe flow and surface overland flow in networks. *Water Sci Technol* 52(5):275–283

- Djordjevic S, Chen A, Leandro J, Savic D, Boonya-aroonnet S, Maksimovic C, Prodanovic D, Blanksby J, Saul A (2007) Integrated sub-surface/surface 1D/1D and 1D/2D modelling of urban flooding. In: Pasche E (ed) Special aspects of urban flood management, Proceedings Cost Session Aquaterra Conference 2007, TUHH, Hamburg, pp 197–207
- Duclos P, Vidonne O, Beuf P, Perray P, Stoebner A (1991) Flash flood disaster—Nîmes, France. *Eur J Epidemiol* 7(4):365–371. doi:10.1007/BF00145001
- Gourbesville P, Savioli J (2002) Urban runoff and flooding: interests and difficulties of the 2D approach. In: Falconer RA, Lin B, Harris EL (eds) *Proceeding of Hydroinformatics 2002*, Cardiff
- Guinot V, Soares-Frazão S (2006) Flux and source term discretization in two-dimensional shallow-water models with porosity on unstructured grids. *Int J Numer Methods Fluids* 50(3):309–345. doi:10.1002/flid.1059
- Haider S, Paquier A, Morel R, Champagne JY (2003) Urban flood modelling using computational fluid dynamics. *Water Marit Eng* 156(2):1–8
- Hirsch C (1988) Numerical computation of internal and external flows: fundamentals of numerical discretization. Wiley, Chichester
- Hsu MH, Chen SH, Chang TJ (2000) Inundation simulation for urban drainage basin with storm sewer system. *J Hydrol (Amst)* 234(1–2):21–37. doi:10.1016/S0022-1694(00)00237-7
- Hubbard ME, Garcia-Navarro P (2000) Flux difference splitting and the balancing of source terms and flux gradients. *J Comput Phys* 165(1):89–125. doi:10.1006/jcph.2000.6603
- Ikeda S, Sato T, Fukuzono T (2008) Towards an integrated management framework for emerging disaster risks in Japan. *Nat Hazards* 44(2):267–280. doi:10.1007/s11069-007-9124-3
- IMPACT (Investigation of Extreme Flood Processes and Uncertainty) (2004) Final Technical Report. Available via [http://www.samui.co.uk/impact-project/IMPACT\\_DetailedTechnicalReport\\_v2\\_2.pdf](http://www.samui.co.uk/impact-project/IMPACT_DetailedTechnicalReport_v2_2.pdf)
- Inoue K, Kawaike K, Hayashi H (2000) Numerical simulation models on inundation flow in urban area. *J Hydrosol Hydraul Eng* 18(1):119–126
- IPCC (2001). Climate change 2001: the scientific basis. Cambridge University Press, Cambridge. Available via [http://www.grida.no/climate/ipcc\\_tar/wg1/index.htm](http://www.grida.no/climate/ipcc_tar/wg1/index.htm)
- Ishigaki T, Nakagawa H, Baba Y (2004) Hydraulic model test and calculation of flood in urban area with underground space. In: Lee JHW, Lam KM (eds) *Proceedings of the 4th international symposium on environmental hydraulics*, Delft
- Lane SN (2005) Roughness: time for a re-evaluation? *Earth Surf Process Landf* 30(2):251–253. doi:10.1002/esp.1208
- Lhomme J, Bouvier C, Mignot E, Paquier A (2006) One-dimensional GIS-based model compared to two-dimensional model in urban floods simulation. *Water Sci Technol* 56(6–7):83–91. doi:10.2166/wst.2006.594
- Marco JB, Cayuela A (1994) Urban flooding: the flood-planned city concept. In: Rossi G, Harmancioglu N, Yevjevich V (eds) *Coping with floods*. Kluwer, Dordrecht, pp 705–721
- Mark O, Weesakul S, Apirumanekul C, Aroonnet SB, Djordjevic S (2004) Potential and limitations of 1-D modelling of urban flooding. *J Hydrol (Amst)* 299(3–4):284–299
- Mignot E (2005) Etude expérimentale et numérique de l'inondation d'une zone urbaine: cas des écoulements dans les carrefours en croix. Dissertation, Université Claude Bernard. Available via <http://www.lyon.cemagref.fr/doc/these/mignot/index.html>
- Mignot E, Paquier A, Ishigaki T (2006a) Comparison of numerical and experimental simulations of a flood in a dense urban area. *Water Sci Technol* 54(6–7):65–73. doi:10.2166/wst.2006.596
- Mignot E, Paquier A, Haider S (2006b) Modeling floods in a dense urban area using 2D shallow water equations. *J Hydrol (Amst)* 327(1–2):186–199. doi:10.1016/j.jhydrol.2005.11.026
- Mingham CG, Causon DM (1998) High-resolution finite-volume method for shallow water flows. *J Hydraul Eng* 124(6):605–614. doi:10.1061/(ASCE)0733-9429(1998)124:6(605)
- Mulet J, Alcrudo F (2003) Uncertainty analysis of Tous flood propagation case study. In: CPS-Universidad de Zaragoza (ed) *Proceedings of the 4rd IMPACT project workshop*, Spain, 2004 (CD-Rom)
- Nania LS (1999) Metodología numerico-experimental para el analisis del riesgo asociado a la escorrentia pluvial en una red de calles. Dissertation, Universitat politecnica de Catalunya
- Nania L, Gómez M, Dolz J (2004) Experimental study of the dividing flow in steep streets crossings. *J Hydraul Res* 42(4):406–412
- Neary VS, Sotiropoulos F, Odgaard AJ (1999) Three-dimensional numerical model of lateral-intake inflows. *J Hydraul Eng* 125(2):126–140. doi:10.1061/(ASCE)0733-9429(1999)125:2(126)
- Nirupama N, Simonovic SP (2007) Increase of flood risk due to urbanisation: a Canadian example. *Nat Hazards* 40(1):25–41. doi:10.1007/s11069-006-0003-0
- Oberle P, Merkel U (2007) Urban flood management-simulation tools for decision makers. In: Ashley R (ed) *Advances in Urban Flood Management*. Taylor and Francis, London, pp 91–112

- Paquier A (1995) Modélisation et simulation de la propagation de l'onde de rupture de barrage. Dissertation, Université Jean Monnet
- Paquier A (1998) 1-D and 2-D models for simulating dam-break waves and natural floods. In: Morris M, Galland JC, Balabanis P (eds) Proceedings of CADAM (Concerted action on dam-break modelling) project, Wallingford, 1998
- Paquier A, Tanguy JM, Haider S, Zhang B (2003) Estimation des niveaux d'inondation pour une crue éclair en milieu urbain: comparaison de deux modèles hydrodynamiques sur la crue de Nîmes d'octobre 1988. *Rev Sci Eau* 16(1):79–102
- Perrin C, Michel C, Andreassian V (2003) Improvement of a parsimonious model for stream flow simulation. *J Hydrol (Amst)* 279(1):1–4. doi:10.1016/S0022-1694(03)00088-X
- Soares-Frazão S, Guinot V (2007) An eigenvector-based linear reconstruction scheme for the shallow-water equations on two-dimensional unstructured meshes. *Int J Numer Methods Fluids* 53(1):23–55. doi:10.1002/flid.1242
- Soares-Frazão S, Zech Y (2007) Experimental study of dam-break flow against an isolated obstacle. *J Hydraul Res* 45(extra issue):27–36
- Testa G, Zuccalà D, Alcrudo F, Mulet J, Soares-Frazão S (2007) Flash flood flow experiment in a simplified urban district. *J Hydraul Res* 45(extra issue):37–44
- Valiani A, Caleffi V, Zanni A (2002) Case study: malpasset dam-break simulation using a 2D finite-volume method. *J Hydraul Eng* 128(5):460–472. doi:10.1061/(ASCE)0733-9429(2002)128:5(460)
- VanLeer B (1979) Towards the ultimate conservative difference scheme. V. A second order sequel to Godunov's method. *J Comput Phys* 32:101–136. doi:10.1016/0021-9991(79)90145-1
- Yoon TH, Kang SK (2004) Finite volume model for two-dimensional shallow water flows on unstructured grids. *J Hydraul Eng* 130(7):678–688. doi:10.1061/(ASCE)0733-9429(2004)130:7(678)
- Yu D, Lane SN (2006) Urban fluvial flood modelling using a two-dimensional diffusion-wave treatment, part 1: mesh resolution effects. *Hydrol Process* 20(7):1541–1565. doi:10.1002/hyp.5935
- Zerger A, Wealands S (2004) Beyond modelling: linking models with GIS for flood risk management. *Nat Hazards* 33(2):191–208. doi:10.1023/B:NHAZ.0000037040.72866.92